Applied Surface Science 258 (2011) 890–897

Contents lists available at SciVerse ScienceDirect

Applied Surface Science

journal homepage: www.elsevier.com/locate/apsusc

Quenching of surface traps in Mn doped ZnO thin films for enhanced optical transparency

Usman Ilyas[a,b], R.S. Rawat[a,*], G. Roshan[a], T.L. Tan[a], P. Lee[a], S.V. Springham[a], Sam Zhang[c], Li Fengji[c], R. Chen[d], H.D. Sun[d]

[a] NSSE, NIE, Nanyang Technological University, 1 Nanyang Walk 637616, Singapore
[b] Department of Physics, University of Engineering & Technology Lahore, Lahore 54890, Pakistan
[c] School of Mechanical and Aerospace Engineering, Nanyang Technological University, 50 Nanyang Avenue 639798, Singapore
[d] Division of Physics and Applied Physics, School of Physical and Mathematical Sciences, Nanyang Technological University, 50 Nanyang Avenue 639798, Singapore

ARTICLE INFO

Article history:
Received 29 June 2011
Received in revised form 1 September 2011
Accepted 6 September 2011
Available online 12 September 2011

Keywords:
ZnO:Mn thin films
Pulsed laser deposition
Photoluminescence
Surface traps
Optical transparency

ABSTRACT

The structural and photoluminescence analyses were performed on un-doped and Mn doped ZnO thin films grown on Si (100) substrate by pulsed laser deposition (PLD) and annealed at different post-deposition temperatures (500–800 °C). X-ray diffraction (XRD), employed to study the structural properties, showed an improved crystallinity at elevated temperatures with a consistent decrease in the lattice parameter 'c'. The peak broadening in XRD spectra and the presence of Mn 2p3/2 peak at ~640 eV in X-ray Photoelectron Spectroscopic (XPS) spectra of the doped thin films confirmed the successful incorporation of Mn in ZnO host matrix. Extended near band edge emission (NBE) spectra indicated the reduction in the concentration of the intrinsic surface traps in comparison to the doped ones resulting in improved optical transparency. Reduced deep level emission (DLE) spectra in doped thin films with declined PL ratio validated the quenching of the intrinsic surface traps thereby improving the optical transparency and the band gap, essential for optoelectronic and spintronic applications. Furthermore, the formation and uniform distribution of nano-sized grains with improved surface features of Mn-doped ZnO thin films were observed in Field Emission Scanning Electron Microscopy (FESEM) images.

1. Introduction

Dilute magnetic semiconductors (DMS) have attracted great research interest due to their promising applications in spintronics. In these materials, the charge and the spin state of electrons are accommodated into a single material leading to interesting magnetic, magneto-optical and magneto-electric properties [1,2]. There has been a considerable interest in the fabrication of semiconducting ZnO for a variety of applications because of their fascinating properties. ZnO, with a direct band gap of 3.37 eV [3], has been found to be a useful candidate material for blue ultraviolet light emitters/detectors, transparent high power electronics and piezoelectric transducers. The low threshold for optical pumping and large exciton binding energy (60 meV) [4,5] allow lasing action in ZnO with extremely low pumping power at room temperature [6] and has been recognized as a promising photonic material in the UV region [7]. The wide band gap of ZnO makes it transparent in the visible range, which is maintained even at higher carrier concentrations, making ZnO a promising material to be used as a transparent conductor. These favorable optical and electrical properties allow ZnO to have wide applications such as transparent electrodes in flat panel displays and solar cells, thin film gas sensors and ultraviolet detectors [8]. Additionally, the high solubility of various 3d transition elements in ZnO makes it suitable for spintronic applications [9,10]. The biggest roadblock in processing of a fully ZnO based device is the unavailability of highly p-type conducting ZnO. The main reason behind the difficulty in achieving p-type conductivity is the presence of surface traps (native defects) such as oxygen vacancies and Zn interstitials which are unintentionally introduced during thin film growth process, making un-doped ZnO inherently an n-type material. So, quenching of surface traps by the incorporation of 3d transition element is essential for ZnO thin films to be used in optoelectronic and spintronic applications.

In this paper, we report the preparation and characterization of un-doped and Mn doped ZnO thin films with enhanced optical transparency due to the quenching of intrinsic surface traps. The wet chemical method [11] was used to synthesize nano-crystalline Mn-doped ZnO powders, which were later pelletized and sintered for making PLD targets. To the best of our knowledge, this method

* Corresponding author. Tel.: +65 6790 3930/3908; fax: +65 6896 9414.
E-mail address: rajdeep.rawat@nie.edu.sg (R.S. Rawat).

0169-4332/$ – see front matter © 2011 Elsevier B.V. All rights reserved.
doi:10.1016/j.apsusc.2011.09.021

has not been used to prepare doped ZnO PLD pellets as the extensive literature search shows the use of solid-state reaction as the main method of preparation of doped PLD pellets. The powder obtained from wet chemical method offers homogeneous doping as compared to the powder obtained by solid-state reaction method. The influence of post-deposition annealing and the dopant concentration on the structural, compositional, photoluminescence and morphological properties of the thin films is investigated and presented.

2. Experimental details

2.1. Preparation of nanocrystalline Mn doped ZnO powder

Nano-crystalline Mn doped ZnO powder with wurtzite structure was synthesized through a wet chemical method. The Mn-doped ZnO powders were prepared for two different Mn doping concentrations of 2 and 5 at.%, hereinafter referred as SP-2% and SP-5%, respectively. The procedure for the preparation of SP-2% powder is as follows: zinc acetate dihydrate (15.79 g), manganese acetate tetrahydrate (0.52 g) and potassium hydroxide (12.96 g) were mixed in 800 ml of methanol. The solution was continuously stirred, using a magnetic stirrer, for 3 h at 52 °C. The solution was then cooled to room temperature and was allowed to age for 24 h to get precipitates. The fine precipitates were removed by centrifugation and washed repeatedly with distilled water to remove unreacted materials. The product was dried in an oven at 50 °C for 1 day. The zinc acetate dihydrate (Aldrich), manganese acetate tetrahydrate (Aldrich), potassium hydroxide (Baker), and methanol (Aldrich), in above mentioned preparation procedure, were used as received. The SP-5% powder was also prepared following the same procedure using suitable quantities of acetates and solvents. The un-doped and Mn dope powders of ZnO were then pelletized under a pressure of 10.5 metric tons and sintered at ~1000 °C for 12 h in air to get PLD targets.

2.2. Pulsed laser deposition (PLD) of thin films

The sintered pellets of Mn doped ZnO were fixed on the gyrating target holder and ablated by second harmonic Nd:YAG laser (532 nm, 26 mJ) at a pulse repetition rate of 10 Hz. The substrate holder was set to rotate at a speed of about 33 rpm to ensure uniform thin film deposition. The thin films were deposited on Si substrate for a constant ablation period of 90 min in ultra high vacuum (10^{-6} Torr). The Si (1 0 0) substrates were sequentially cleaned in ultrasonic bath with ethanol, acetone and de-ionized water, separately, at a temperature of 45 °C for 15 min each, before being mounted to the substrate holder in the PLD chamber. Deposited thin films were annealed at different temperatures (500, 600, 700 and 800 °C) for 4 h in air.

The crystalline phase of thin films was analyzed using a SIEMENS D5005 Cu Kα (1.504 Å) X-ray Diffractometer (XRD). Near band edge (NBE) energy transitions in Photoluminescence (PL) spectra, measured using Hd–Cd (325 nm, 10 mW) laser, were used to study the variation in surface traps (intrinsic defects) and optical band gap with dopant concentration. X-ray Photoelectron Spectroscopy (XPS) with Kratos Axis-Ultra Spectrometer, equipped with a focused monochromatic Al-Kα (1486.6 eV) X-ray beam (15 kV and 10 mA), was used to identify the surface stoichiometry and elemental oxidation states of thin film samples. The morphology of thin films was characterized using a Joel JSM 6700 Field Emission Scanning Electron Microscope (FESEM).

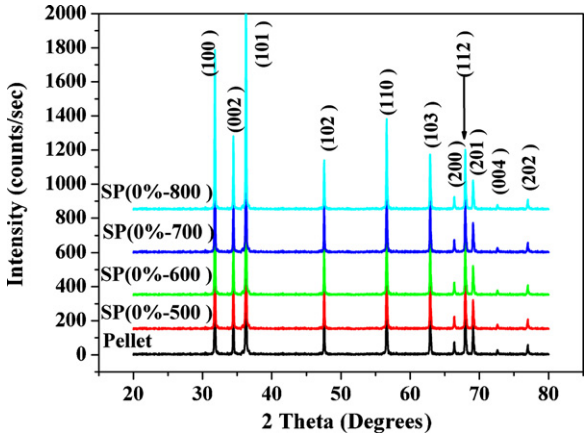

Fig. 1. XRD spectra of polycrystalline SP-0% ZnO thin films annealed at different temperatures (500–800 °C).

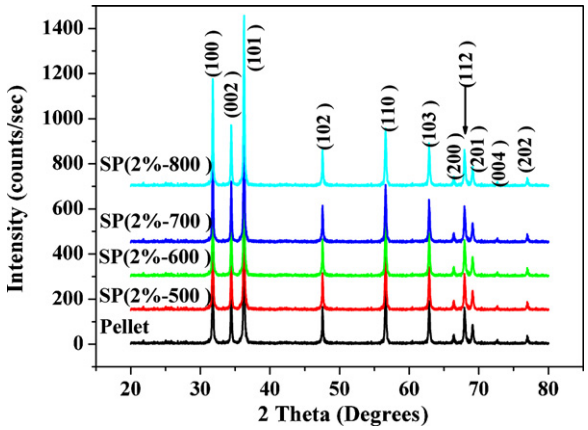

Fig. 2. XRD spectra of SP-2% ZnO thin films annealed at different temperatures (500–800 °C).

3. Results and discussion

3.1. Structural analysis

The XRD spectra of ZnO thin films doped with different Mn concentrations and annealed at 500–800 °C are shown in Figs. 1–3. The XRD peaks corresponding to (1 0 0), (0 0 2), (1 0 1), (1 0 2), (1 1 0),

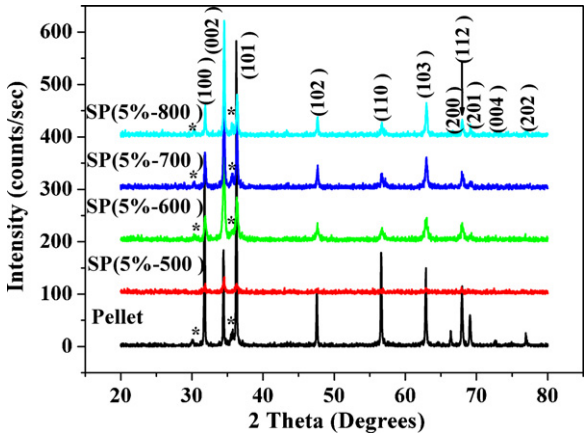

Fig. 3. XRD spectral profiles of SP-5% ZnO thin films annealed at different post-deposition annealing temperatures (500–800 °C) showing the formation of $Zn_2Mn_3O_8$ impurity phases.

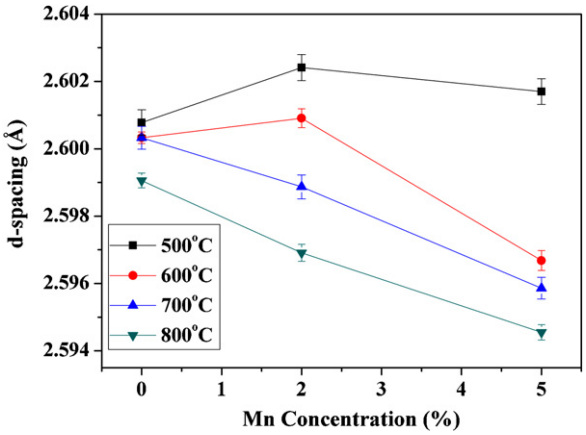

Fig. 4. Variation in d-spacing in un-doped and Mn-doped ZnO thin films annealed at 500, 600, 700 and 800 °C.

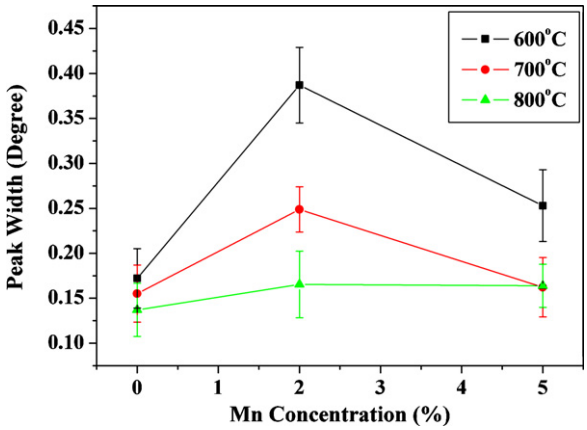

Fig. 5. Variation in diffraction peak width as a function of Mn content and post-deposition annealing temperature.

(1 0 3), (2 0 0), (1 1 2), (2 0 1) and (2 0 2) diffraction planes of wurtzite ZnO are observed in 2θ range from 20° to 80° for all thin film samples indicating polycrystalline nature. The obtained XRD spectra matched well with the space group $P6_3mc$ (186) (No. 36-1451) of wurtzite ZnO structure.

The XRD spectra shown in Fig. 2, for sintered pellet and annealed thin films with 2 at.% Mn doping, do not show any impurity phases. However, diffraction peaks corresponding to spinal structures of Mn doped ZnO are observed in the pellet and thin films of SP-5% samples indicating the formation of impurity phases (marked by *) at higher doping concentrations as shown in Fig. 3. The observation of similar phases in pellets and corresponding thin films confirms the ability of PLD to maintain the stoichiometery of the material from the pellet to the thin film. The secondary phases are identified as the spinal structure of $Zn_2Mn_3O_8$ having space group *Pmn*21 (31) (No. 32-1472). The signatures of manganese acetate are not observed in our samples indicating the absence of any un-reacted Mn in the thin film samples.

The texture coefficient of the thin films was calculated to determine the preferred orientation of the polycrystalline thin films using the formula proposed by Barrett and Massalski [12]. The (0 0 2) peak was found to have the highest texture coefficient indicating the preferred orientation of the films along this plane. Hence, the parameters such as diffraction peak shift, average crystallize size, peak width and lattice parameter 'c' were estimated for this diffraction peak.

Highly textured (0 0 2) peak, centered at about 34.42° (characterizing the hexagonal wurtzite structure), was found to shift towards smaller/larger angles for Mn doped thin films in comparison to un-doped ones indicating the increase/decrease in d-spacing as is evident from Fig. 4. The peak shift in XRD spectra, obtained at different temperatures, reveals the substitution of Mn in its different oxidation states [13]. The peak shift towards smaller angles for SP-2% samples annealed at 500 and 600 °C suggests the increase in d-spacing due to the substitution of Zn^{2+} ions (0.60 Å) by larger sized Mn^{2+} ions (0.66 Å) in ZnO. However, the decrease in d-spacing for SP-5% samples might be due to the substitution of Zn^{2+} ions by the Mn ions of smaller radii (Mn^{4+} and Mn^{3+} ions have ionic radii of 0.53 and 0.58 Å, respectively) in ZnO host matrix [14]. A general trend observed in Fig. 4, for both the doping concentrations, is the decrease in d-spacing with the increase in annealing temperature pointing to the increase in the relative amount of Mn^{4+} or Mn^{3+} ions as compared to that of Mn^{2+} ions.

The variations in peak width (FWHM) of (0 0 2) diffraction peak, with the increase in Mn doping concentration for different annealing temperatures, are shown in Fig. 5. The un-doped ZnO thin film sample (SP-0%) exhibits a narrow FWHM compared to the SP-2% and SP-5% samples. The peak broadening in doped samples is attributed to the incorporation of Mn at the substitutional sites of Zn. The average crystallite size, estimated from FWHM of the diffraction peaks using Scherrer formula, was calculated to be 20, 23 and 26 nm for SP-0%; 9, 14 and 21 nm for SP-2% and 14, 22 and 22 nm for SP-5% samples annealed at 600, 700 and 800 °C, respectively. The reduced values of the lattice parameters indicate the deterioration in crystallinity of ZnO thin films due to Mn doping. The decrease in average crystallite size due to Mn content is also reported in literature [15,16]. However, in our case the average crystallite size increased with annealing temperature for un-doped and doped samples as observed by other researchers as well [16,17].

The value of lattice parameter 'c' decreased with an increase in annealing temperature, as seen in Fig. 6. This decrease in lattice parameter is attributed to zinc vacancies [18] which are produced in large number at elevated temperatures [19]. Theoretical investigations, by Khalid et al. [18], have confirmed the reduction in lattice parameter due to zinc vacancies. Furthermore, during the annealing of ZnO coated silicon wafer, ZnO atoms of the films are arranged by the thermal energy which leads to a reduction in the tensile stress. A compressive stress will be generated by silicon when substrate temperature drops from annealing temperature to room temperature during the cooling cycle of the annealed sample. The compressive stresses of silicon and ZnO film will cancel out each other. However, for very high (700–800 °C) annealing

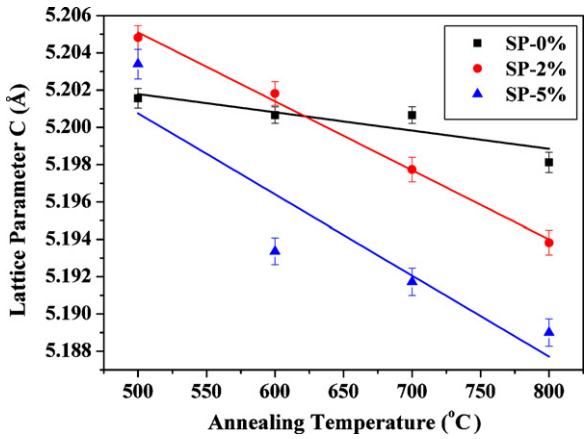

Fig. 6. Variation in lattice parameter 'c' of SP-0%, SP-2% and SP-5% samples with annealing temperature.

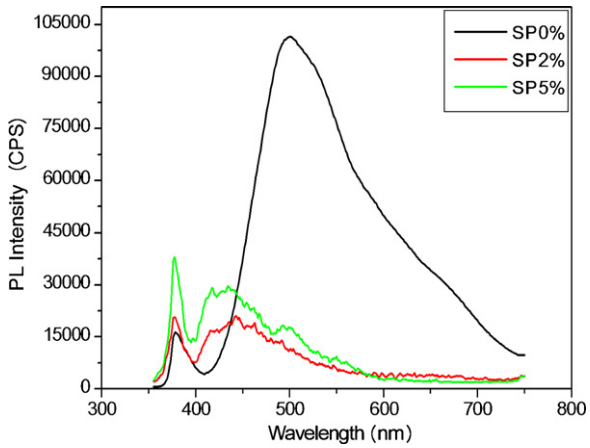

Fig. 7. Room temperature PL emission spectra, consisting of near band edge and deep level emission bands, of un-doped and Mn doped ZnO thin films annealed at 600 °C.

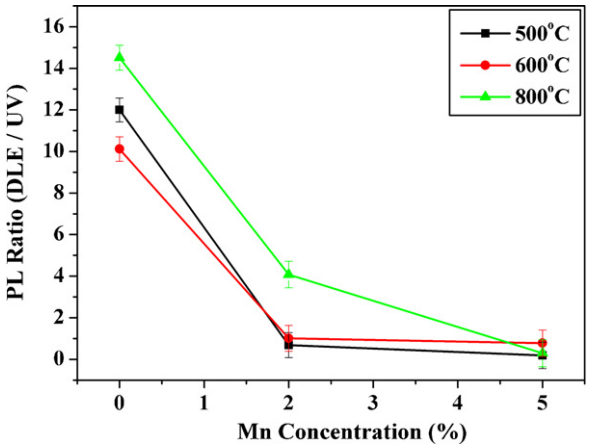

Fig. 8. Variation in PL ratio (ratio of DLE to UV emission peak intensities) as a function of Mn concentration at different annealing temperatures.

temperatures, the compressive stress will be higher than the tensile stress [20] ultimately reducing the lattice parameter of the crystal.

Fig. 6 shows that at a fixed annealing temperature of 500 °C the lattice parameter 'c' in doped samples is higher than that of the un-doped sample. This could be due to the incorporation of 0.66 Å sized tetrahedral Mn^{2+} ion at the substitutional sites of 0.60 Å sized Zn^{2+} ion [21] leading to a tensile stress in thin films. The tensile stress, indicated by increase in lattice parameter 'c', in the ZnO thin film can also be attributed to the zinc and oxygen interstitials [22,23]. At higher temperature of 700 and 800 °C, the trend is reversed, i.e. the doped samples have smaller lattice parameter as compared to un-doped samples that may be attributed to the incorporation of smaller amount of Mn^{2+} ions at the substitutional sites of Zn^{2+} at elevated temperatures. This observation will be further explained on the basis of XPS results in Section 3.3.

3.2. Photoluminescence analysis

The room temperature PL analysis was carried out to study the effect of Mn content and the annealing temperature on the structural defects and the band gap energy of ZnO thin films. PL spectra of un-doped and Mn doped ZnO thin films exhibit two emission spectra in UV (at ~380 nm) and deep level (mostly in the green and partly in the yellow and red spectral regions) bands. In our case, the UV band emission, centered at ~380 nm, is originated from the exciton recombination corresponding to the near band edge (NBE) exciton emission of the wide band gap ZnO. This recombination takes place through an exciton–exciton collision process at room temperature [24]. While the deep level emission (DLE) spectrum [25–27], which strongly manifests a polycrystalline structure [28] of ZnO, is due to a high density of native defects such as zinc vacancy (V_{Zn}), oxygen vacancy (V_O), interstitial zinc (Zn_i) and interstitial oxygen (O_i). The contribution of native (due to zinc and oxygen) and foreign (due to manganese) defects on PL spectrum can be evaluated by the estimation of relative intensities of the deconvoluted peaks.

Fig. 7 shows the typical room temperature PL spectra of un-doped and Mn doped thin films annealed at 600 °C. It may be noted that similar spectral features were observed for samples annealed at other temperatures. The deconvolution of broad DLE peak was used to estimate the relative contribution of native and foreign defects. The DLE spectrum in green and yellow region for SP-0%, was deconvoluted into three peaks centered at 491.9, 545.8 and 652.1 nm (deconcoluted peaks are not shown), which are attributed to the contribution from a singly ionized V_{Zn} (31.8%), V_O (41.6%) and O_i (24.4%) respectively. Strong DLE spectrum for un-doped sample indicates the increased concentration of native (zinc and oxygen vacancy) defects in comparison to doped ones. For doped samples, the DLE emission spectrum can be attributed to both native (intrinsic) and foreign (extrinsic) defects. Mn related (foreign) defects were estimated to be the dominant defects in SP-5% samples as the contribution from native defects (zinc and oxygen vacancies) was relatively low. The emission in the range of 420–470 nm is reported to be due to the presence of Mn ions in ZnO host matrix [29]. Mn related extrinsic defects (with deconvoluted DLE peak at about 428–434 nm) were dominant in SP-5% thin films. Their contribution in SP-2% thin films was negligible. This could be attributed to the formation of spinal phase of $Zn_2Mn_3O_8$ in SP-5% thin films.

Fig. 8 shows a marked decrease in the ratio of DLE to UV emission peaks (PL ratio) with increasing Mn concentration. As the DLE peak is associated with the intrinsic surface traps (defects), the relative decrease in DLE emission peak indicates the quenching of intrinsic surface traps at higher Mn doping concentration. At the same time, the increase in UV emission peak intensity (at ~380 nm) for doped samples, as seen in Fig. 7, reveals the improved optical transparency which is essential for transparent high power electronics and transparent conductive thin films [30]. This indicates that the controlled Mn doping of ZnO can enhance the optical properties of ZnO for applications in optoelectronics, in addition to its usual application in the field of spintronics.

The deconvoluted DLE peak at about 500 nm for SP-5% sample (not shown here) indicates the contribution of intrinsic defects related to V_{Zn}, which are calculated to be 30%, 27% and 13% at annealing temperatures of 500, 600 and 700 °C, respectively. No signatures of Zn_i were observed at 800 °C for SP-5% sample. For SP-2% samples, the maximum contribution towards the structural defects is attributed to the doubly ionized zinc vacancies, which show a deconvoluted DLE emission peak at about 463 nm. The concentration of Zn vacancies was calculated to be 71%, 50%, 45% and 61% at annealing temperatures of 500, 600, 700 and 800 °C, respectively.

The shift of UV emission peak as a function of annealing temperature for SP-5% samples was estimated and is shown in Fig. 9(a). It was observed that the UV peak shifts towards longer wavelength (i.e. shorter energy from 3.28 eV to 3.27 eV) for SP-5% thin films with an increase in temperature. Similar behavior was observed for SP-0% (3.24–3.0 eV) and SP-2% (3.28–3.27 eV), which is in agreement with the results reported by Wang et al. [31]. This red shift can be partially explained by the shrinkage of the energy band gap with an increase in particle size [32]. The increased particle size due to grain growth at higher annealing temperatures will result in larger number of atoms in the particle causing the greater splitting of energy

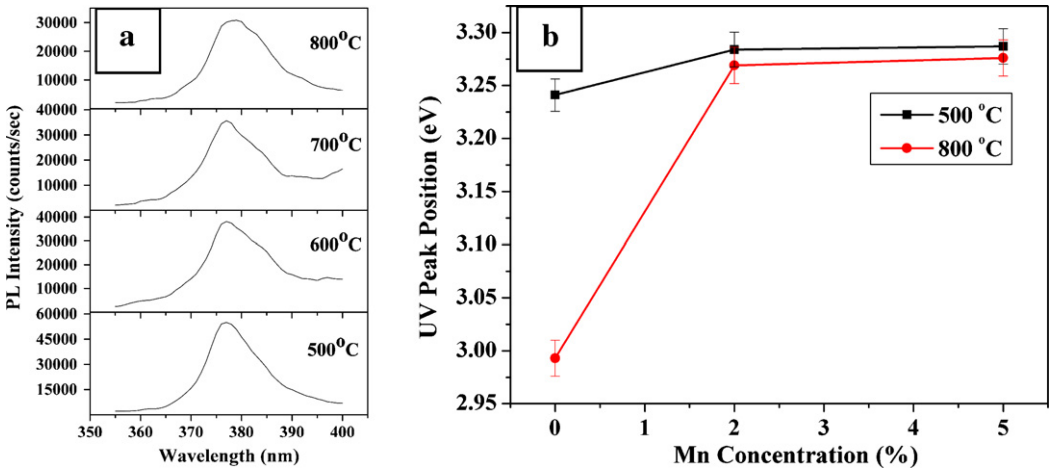

Fig. 9. UV peak shift, in PL emission spectra, of SP-5% thin film (a) with annealing temperature and (b) with Mn concentration.

levels resulting in the shrinkage of the energy band gap. The grain growth at higher annealing temperatures was also consistent with our XRD results. Moreover, the contribution of intrinsic and extrinsic defects with the increase in annealing temperature, can also lead to the shrinkage of the energy band gap of ZnO.

The samples annealed at a given temperature, however, show the UV emission peak shift towards the shorter wavelength (blue shift) side with the increase in Mn content, as is evident from Fig. 9(b) which exhibits the trend for two extreme annealing temperatures used. The observed blue shift in UV emission peak with Mn doping can be attributed to the observed decrease in average crystallite size of Mn doped ZnO leading to broadening of energy band gap, which is consistent with XRD results.

3.3. Compositional analysis

The compositional analysis of ZnO thin films was performed using XPS by investigating the Zn 2p, Mn 2p and O 1s core level spectra. The binding energies were calibrated by the adventitious carbon C 1s peak (284.6 eV). The main XPS spectra of ZnO exhibit a core level binding energy peak of Zn $2p_{3/2}$ located at 1022.0 eV, as shown in Fig. 10. The Zn $2p_{3/2}$ spectrum exhibits slightly asymmetrical features indicating the possibility of existence of multi-component Zn. A Gaussian peak fitting was performed to analyze the electronic/oxidation states of Zn. The deconvoluted peaks of Zn $2p_{3/2}$ of SP-0%, SP-2% and SP-5% annealed at 700 °C are shown in Fig. 10.

The deconvoluted peaks of Zn $2p_{3/2}$ of SP-0% annealed at 700 °C, shown in Fig. 10(a), are centered at 1020.4, 1022.2 and 1023.2 eV. The peak centered at 1022.2 eV represents the Zn^{2+} ions in stoichiometric ZnO [33] while the peak at 1023.2 eV might be related to the native zinc vacancies which have been observed in the materials annealed at elevated temperatures [34]. The lower energy peak at 1020.4 eV is attributed to the loss in the number of oxygen ions in nano-crystalline ZnO [33]. It will reduce the charge transfer from zinc to oxygen thus increasing the shielding effect of the valence electrons in Zn ions which decreases the binding energy of the core electrons in the Zn ion. Thus, the deconvoluted XPS peaks at lower and higher energies in un-doped samples verify the presence of native zinc and oxygen vacancy defects which is also inferred through the PL analysis.

The Zn $2p_{3/2}$ peak for SP-2% sample, as shown in Fig. 10(b), was deconvoluted with two peaks centered at about 1019.51 and 1021.21 eV. The peak corresponding to Zn^{2+} ions in stoichiometric ZnO, normally observed at about 1022 eV, shifted to the lower binding energy of 1021.21 eV. This shift in binding energy is due to the partial substitution of Zn in ZnO lattice by Mn^{2+} ions and Zn–Mn bonding structure [35]. In addition, the different bonding states of the elements in the surface will result in a shift in the binding energy towards lower value. Since the electro negativity of Mn ($\chi = 1.55$) is smaller than that of O ($\chi_O = 3.44$) [36], Zn atoms bonded to the Mn atoms will contribute to shift in the binding energy of Zn $2p_{3/2}$ peak. Furthermore, the reduced average crystallite size, which broadens the peak, also contributes to the shift in the binding energy towards the lower energy side [33] that is consistent with our XRD results.

Fig. 10(c) shows the deconvoluted peaks of Zn $2p_{3/2}$ peak of SP-5% sample annealed at 700 °C. The deconvoluted peaks are centered at about 1020.64, 1022.34 and 1023.16 eV. Earlier, the PL analysis has established that the concentration of structural defects for SP-5% thin films are lower than that of un-doped ones so the peak shift towards the higher binding energy value due to V_{Zn} is ruled out in this case. The deconvoluted peak centered at about 1023.16 eV

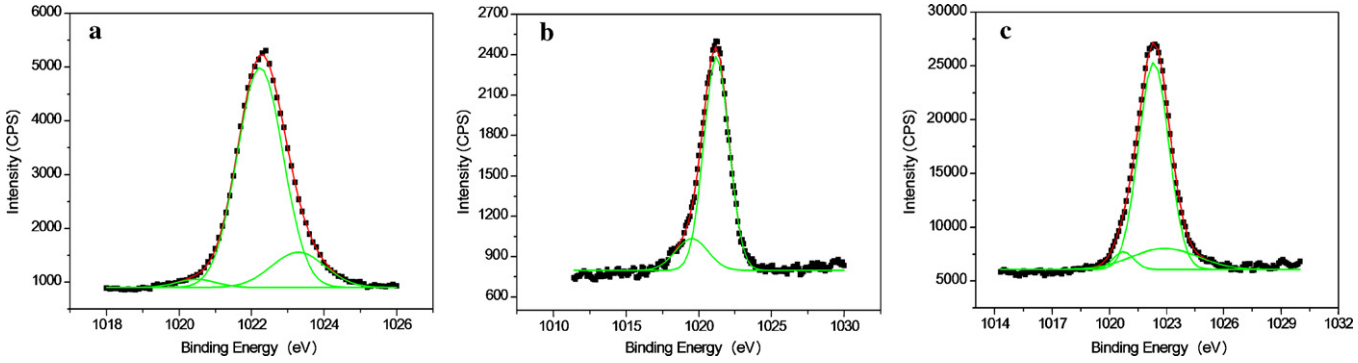

Fig. 10. XPS core level spectra of Zn 2p3/2 peak, deconvoluted with Gaussian peaks, for (a) SP-0%, (b) SP-2% and (c) SP-5% thin films annealed at 700 °C.

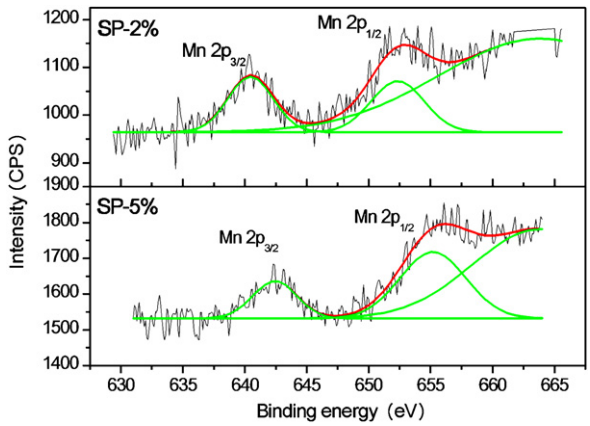

Fig. 11. Mn 2p core level XPS spectra, deconvoluted using Gaussain peak fitting, of SP-2% and SP-5% thin film samples annealed at 800 °C.

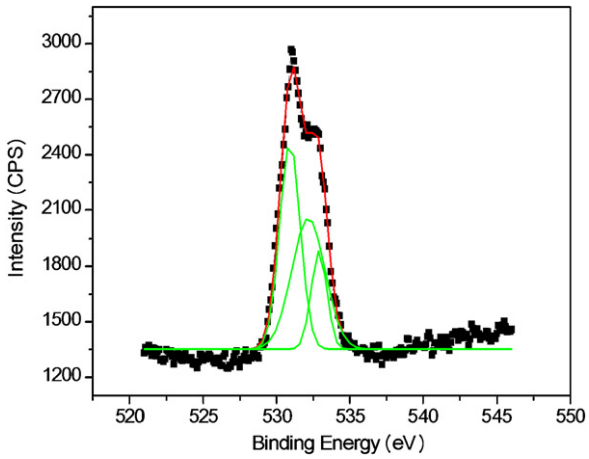

Fig. 12. O1 s core level XPS spectrum, deconvoluted with three peaks centered at 531.0, 532.1 and 532.8 eV, of SP-5% thin film annealed at 800 °C.

is attributed to the Zn in $Zn_2Mn_3O_8$. This is because the atoms of higher positive oxidation state (Mn^{4+} in $Zn_2Mn_3O_8$ phase) exhibit a higher binding energy due to extra columbic interaction between the photo-emitted electron and the ion core. The appearance of this phase is also confirmed from our XRD results.

Fig. 11 reveals that the binding energies of Mn $2p_{3/2}$ for SP-2% and SP-5% ZnO thin films are centered at about 640.4 and 642.4 eV showing that the Mn ions in the films are mainly in the chemical states of Mn^{2+} and Mn^{4+} [36,37] respectively, which is also consistent with the peak shift observed in XRD spectra. Moreover, the binding energy of Mn $2p_{3/2}$ shifts towards the lower energy side in comparison to commercial MnO powders (640.7 eV), which is related to the incorporation of Mn^{2+} ions into the lattice sites of Zn in ZnO [38]. The concentration of Mn^{2+} in SP-2% thin films, calculated from the relative area under the curves of deconvoluted peaks of Mn $2p_{3/2}$, reduced from 28.5 to 21.5% with the increase in annealing temperature. The reduction in concentration of Mn^{2+} ions with the increase in annealing temperature could result in the contraction of ZnO lattice ultimately leading to a reduction in lattice parameter, as is evident from the analysis of XRD results.

The asymmetric O 1s XPS peak was deconvoluted with peaks centered at about 531.0, 532.1 and 532.8 eV respectively for the thin films annealed at 800 °C as shown in Fig. 12. However, the peak centered at ~530 eV was also observed for thin films that were annealed at lower temperatures. The results are almost similar to that of Chen et al. and Wang et al. [39,40], who attributed this peak to the O^{2-} ions on the wurtzite structure of the hexagonal Zn^{2+} ion array. Based on these reports, the lower energy peak of oxygen spectrum is attributed to Zn–O bonds [41] which are dominant in the thin films annealed at lower temperatures.

The higher binding energy peak (at 532.1 or 532.8 eV) is usually attributed to the chemisorbed or dissociated oxygen or hydroxyl (OH) species on the surface of the ZnO thin film, such as CO_3, adsorbed H_2O or O_2 [42]. The component at the medium binding energy (531.0 eV) is associated with the O^{2-} ions that are in oxygen deficient regions within the ZnO matrix and is related to actual O 1s contribution of the samples. The presence as well as the changes in the intensity of this component may be related, in parts, to the variation in the concentration of oxygen vacancies [43]. The calculation of the concentration of oxygen vacancies showed a reduction from 60% for un-doped samples to 35% in doped samples annealed at 800 °C. The reduction in this component also verifies the PL emission spectrum that showed a reduction in the native defects with Mn incorporation.

3.4. Morphological studies

The surface morphologies of the Mn doped ZnO thin films, all annealed at 600 °C, are shown in Fig. 13. Different morphologies of Mn doped ZnO thin films at different Mn concentrations are observed. The surface features of SP-0% thin film reveal the presence of rod like structures. For SP-2% sample, the film consists of agglomerated grains and hence grain boundaries cannot be distinguished clearly. However, regular grains can be seen clearly in SP-5% thin films having uniform size distribution in the range of about 85–95 nm. The value of grain size is larger than that calculated from XRD. Higher grain size might be attributed to the migration of grain boundaries causing the coalescence of smaller grains at higher annealing temperature. Furthermore, the surface

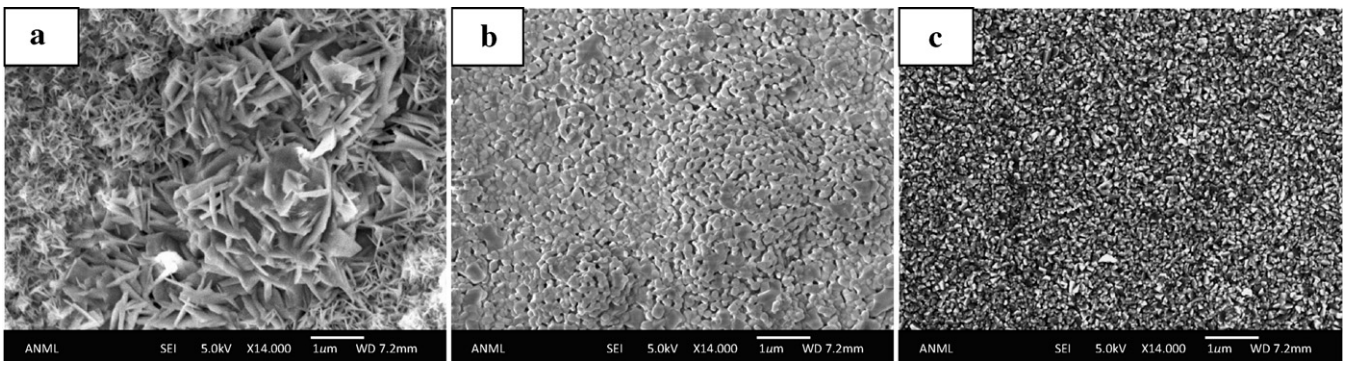

Fig. 13. FESEM micrograph showing the surface morphology of (a) SP-0%, (b) SP-2% and (c) SP-5% thin films annealed at 600 °C.

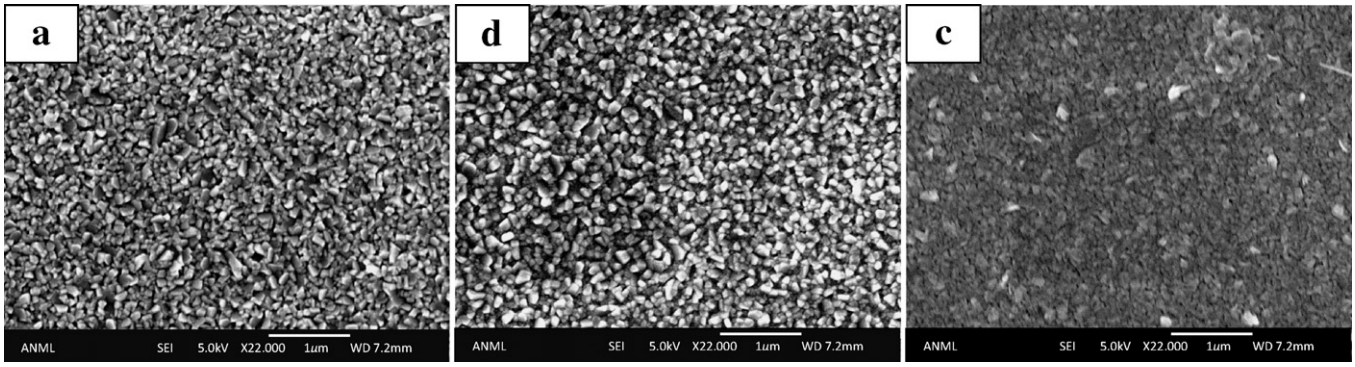

Fig. 14. FESEM micrograph showing the surface morphology of SP-5% sample annealed at (a) 600 °C, (b) 700 °C and (c) 800 °C.

topography of ZnO thin films becomes smoother with increase in Mn content, as Mn incorporation causes regular grain size resulting in the formation of more uniform thin films [43].

Fig. 14 shows the changes in surface morphologies of SP-5% thin films with the annealing temperature. Clearly distinguished grains are observed on samples annealed at 600 and 700 °C with slight increase in the grain size. With further increase in the annealing temperature to 800 °C, the grain size appears to be similar but with a dense packing due to coalescence of neighboring grains.

4. Conclusions

Nanocrystalline ZnO and ZnO:Mn powders were successively prepared by a simple wet chemical method using zinc and manganese acetates as precursors instead of commonly used solid-state reaction method. The powders were then pressed and sintered to make target pellets for PLD. The thin films of ZnO and ZnO:Mn, grown by PLD and annealed at different temperatures, showed interesting structural, optical, compositional and morphological properties. The XRD spectra showed the improved crystalline quality of the thin films at elevated annealing temperatures without any degradation in the wurtzite structure of ZnO. A reduction in average crystallite size and the peak broadening of the doped samples pointed to the successful incorporation of Mn in ZnO lattice. Furthermore, the detailed analysis of XPS core level peaks of Zn and Mn illustrates the presence of Zn^{2+}, Mn^{2+} and Mn^{4+} ions in the wurtzite structure of ZnO thin films. The FESEM revealed the existence of well-defined nano-sized (85–95 nm) grains in Mn doped thin films with improved film quality and smoother surface features at elevated temperatures. One of the major findings from the PL spectra is the marked decrease in PL (DLE to UV emission peak) ratio with the significant increase in the intensity of near band edge UV emission peak at higher Mn doping concentrations indicating thereby the quenching of surface traps and enhanced optical transparency. The controlled Mn doping of ZnO therefore leads to the enhancement in the optical transmission properties of ZnO thin films which is desirable for its applications in optoelectronics, in addition to its usual application in the field of spintronics.

Acknowledgments

The authors are grateful to the National Institute of Education, Nanyang Technological University Singapore, for providing the AcRF grant RI 7/08 RSR. One of us, Usman Ilyas, would like to thank University of Engineering & Technology Lahore for providing the fully funded research scholarship under Faculty Development Program (FDP) of Higher Education Commission of Pakistan.

References

[1] S.A. Wolf, D.D. Awschalom, R.A. Buhrman, J.M. Daughton, S.V. Molnar, M.L. Roukes, A.Y. Chtchelkanova, D.M. Treger, Spintronics: a spin-based electronics vision for the future, Science 294 (2001) 1488–1495.
[2] H. Ohno, Making nonmagnetic semiconductors ferromagnetic, Science 281 (1998) 951–956.
[3] Y. Ohta, T. Haage, Y. Abe, Crystallographic features of ZnO single crystal, Jpn. J. Appl. Phys. 36 (1997) L1040–L1042.
[4] D.C. Look, Recent advances in ZnO materials and devices, Mater. Sci. Eng. B 80 (2001) 383–387.
[5] D.C. Reyonlds, D.C. Look, B. Jogai, C.W. Liton, G. Gantwell, W.C. Harsh, Valence-band ordering in ZnO, Phys. Rev. B 60 (1999) 2340–2344.
[6] U. Ozgur, Y.I. Alivov, C. Liu, A. Teke, M.A. Reshcchikov, S. Dogan, V. Avrutin, S.J. Cho, H. Morkoe, A comprehensive review of ZnO materials and devices, J. Appl. Phys. 98 (2005) 41301–41403.
[7] K.J. Ko, Y.F. Chen, T. Yao, I. Kobayashi, H. Uchiki, Photoluminescence properties of ZnO epilayers grown on CaF_2(111) by plasma assisted molecular beam epitaxy, Appl. Phys. Lett. 76 (2000) 1905–1907.
[8] P. Sharma, K. Sreenivas, K.V. Rao, Analysis of ultraviolet photoconductivity in ZnO films prepared by unbalanced magnetron sputtering, J. Appl. Phys. 93 (2003) 3963–3970.
[9] Z. Jin, T. Fukumura, M. Kawasaki, K. Ando, H. Saito, T. Sekiguchi, Y.Z. Yoo, M. Murakami, Y. Matsumoto, T. Hasegawa, H. Koinuma, High throughput fabrication of transition-metal-doped epitaxial ZnO thin films: a series of oxide-diluted magnetic semiconductors and their properties, Appl. Phys. Lett. 78 (2001) 3824–3826.
[10] Z. Jin, M. Murakami, T. Fukumura, Y. Matsumoto, A. Ohtomo, M. Kawasaki, H. Koinuma, Combinatorial laser MBE synthesis of 3d ion doped epitaxial ZnO thin films, J. Cryst. Growth 214 (2000) 55–58.
[11] L. Vayssieres, K. Keis, S.E. Lindquist, A. Hagfledt, Purpose-built anisotropic metal oxide material: 3D highly oriented microrod array of ZnO, J. Phys. Chem. B 105 (2001) 3350–3352.
[12] C. Barret, T.B. Massalski, Structure of Metals, Pergamon, Oxford, 1980.
[13] P. Sharma, A. Gupta, F.J. Owens, A. Inoue, K.V. Rao, Room temperature spintronic material Mn-doped ZnO revisited, J. Magn. Magn. Mater. 282 (2004) 115–121.
[14] N. Theodoropolou, V. Misra, J. Philip, P. Leclair, G.P. Berera, J.S. Moodera, B. Satpati, T. Som, High-temperature ferromagnetism in $Zn_{1-x}Mn_xO$ semiconductor thin films, J. Magn. Magn. Mater. 300 (2006) 407–411.
[15] J. Luo, J.K. Liang, Q.L. Liu, F.S. Liu, Y. Zhang, B. Sun, G.H. Rao, Structure and magnetic properties of Mn-doped ZnO nanoparticles, J. Appl. Phys. 97 (2005) 86106–86108.
[16] S. Deka, P.A. Joy, Synthesis and magnetic properties of Mn doped ZnO nanowires, Solid State Commun. 142 (2007) 190–194.
[17] X.J. Liu, C. Song, F. Zhang, X.B. Wang, F. Pan, Influence of annealing on microstructure and magnetic properties of co-sputtered Co-doped ZnO thin films, J. Phys. D: Appl. Phys. 40 (2007) 1608–1613.
[18] M. Khalid, M. Ziese, A. Setzer, P. Esquinazi, et al., Defect-induced magnetic order in pure ZnO films, Phys. Rev. B 80 (2009) 035331–035335.
[19] S. Dutta, S. Chattopadhyay, D. Jana, A. Banerjee, S. Manik, S.K. Pradhan, M. Sutradhar, A. Sarkar, Annealing effect on nano-ZnO powder studied from positron lifetime and optical absorption spectroscopy, J. Appl. Phys. 100 (2006) 114328–114333.
[20] M. Jung, J. Lee, S. Park, H. Kim, J. Chang, Investigation of the annealing effects on the structural and optical properties of sputtered ZnO thin films, J. Cryst. Growth 283 (2005) 384–389.
[21] G. Lawes, A.S. Risbud, A.P. Ramirez, R. Seshadri, Absence of ferromagnetism in Co and Mn substituted polycrystalline ZnO, Phys. Rev. B 71 (2005) 45201–45205.
[22] C. Hanhong, L. Jianguo, Y. Zhizhen, W. Lei, Z. Binghui, The effects of thermal annealing on ZnO thin films by reactive magnetron sputtering, Vac. Sci. Technol. (China) 22 (2002) 467–469.

[23] Z.B. Fang, Z.I. Yan, Y.S. Tan, X.Q. Liu, Y.Y. Wang, Influence of post-annealing treatment on the structure properties of ZnO films, Appl. Surf. Sci. 241 (2005) 303–308.
[24] L.L. Yang, Q.X. Zhao, M. Willander, J.H. Yang, I. Ivanov, Annealing effects on optical properties of low temperature grown ZnO nanorod arrays, J. Appl. Phys. 105 (2009) 53503–53509.
[25] B. Lin, Z. Fu, Y. Yia, Green luminescent center in undoped zinc oxide films deposited on silicon substrates, Appl. Phys. Lett. 79 (2001) 943–945.
[26] K. Vanheusden, W.L. Warren, C.H. Seager, D.K. Tallant, J.A. Voigt, B.E. Gnade, Mechanisms behind green photoluminescence in ZnO phosphor powders, J. Appl. Phys. 79 (1996) 7983–7990.
[27] M. Liu, A.H. Kitai, P. Mascher, Point defects and luminescence centres in zinc oxide and zinc oxide doped with manganese, J. Lumin. 54 (1992) 35–42.
[28] S.M. Abrarov, S.U. Yuldashev, T.W. Kim, Y.H. Kwon, T.W. Kang, Deep level emission of ZnO nanoparticles deposited inside UV opal, Opt. Commun. 259 (2006) 378–384.
[29] R. Viswanatha, S. Sapra, S.S. Gupta, B. Satpati, P.V. Satyam, B.N. Dev, D.D. Sarma, Synthesis and characterization of Mn-doped ZnO nanocrystals, J. Phys. Chem. B 108 (2004) 6303–6310.
[30] Q.P. Wang, D.H. Zhang, Z.Y. Xue, X.J. Zhang, Mechanisms of green emission from ZnO films prepared by rf magnetron sputtering, Opt. Mater. 26 (2004) 23–26.
[31] Y.G. Wang, S.P. Lau, H.W. Lee, S.F. Yu, B.K. Tay, Photoluminescence study of ZnO films prepared by thermal oxidation of Zn metallic films in air, J. Appl. Phys. 94 (2003) 354–358.
[32] A.V. Dijkin, E.A. Meulenkamp, D. Vanmaekelbergh, A. Meijerink, Identification of the transition responsible for the visible emission in ZnO using quantum size effects, J. Lumin. 90 (2000) 123–128.
[33] Y.Y. Taya, S. Lib, C.Q. Sun, P. Chen, Size dependence of Zn 2*p* 3/2 binding energy in nanocrystalline ZnO, Appl. Phys. Lett. 88 (2006) 173118–173120.
[34] A. Kelly, G.W. Groves, P. Kidd, Crystallography and Crystal Defects, Wiley, New York, 2000.
[35] C.J. Cong, L. Liao, J.C. Li, L.X. Fan, K.L. Zhang, Synthesis, structure and ferromagnetic properties of Mn-doped ZnO nanoparticles, Nanotechnology 16 (2005) 981–984.
[36] W. Xiao, Q. Chen, Y. Wu, T. Wu, L. Dai, Ferromagnetism of $Zn_{0.95}Mn_{0.05}O$ controlled by concentration of zinc acetate in ionic liquid precursor, Mater. Chem. Phys. 123 (2010) 1–4.
[37] J.F. Moulder, W.F. Stickle, P.E. Sobol, K.D. Bomben, Handbook of X-ray Photoelectron Spectroscopy, Eden, Prairie, 1995.
[38] Y. Guo, X. Cao, X. Lan, C. Zhao, X. Xue, Y. Song, Solution-based doping of manganese into colloidal ZnO nanorods, J. Appl. Phys. Chem. C 112 (2008) 8832–8838.
[39] M. Chen, X. Wang, Y.H. Yu, Z.L. Pie, X.D. Bai, C. Sun, R.F. Huang, L.S. Wen, X-ray photoelectron spectroscopy and auger electron spectroscopy studies of Al-doped ZnO films, Appl. Surf. Sci. 158 (2000) 134–140.
[40] Z.G. Wang, X.T. Zu, S. Zhu, L.M. Wang, Green luminescence originates from surface defects in ZnO nanoparticles, Physica E 35 (2006) 199–202.
[41] J.H. Li, D.Z. Shen, J.Y. Zhang, D.X. Zhao, B.S. Li, Y.M. Lu, Y.C. Liu, X.W. Fan, Magnetism origin of Mn-doped ZnO nanoclusters, J. Magn. Magn. Mater. 302 (2006) 118–121.
[42] S. Major, S. Kumar, M. Bhatnagar, K.L. Chopra, Effect of hydrogen plasma treatment on transparent conducting oxides, Appl. Phys. Lett. 49 (1986) 394–396.
[43] T. Szorenyi, L.D. Laude, I. Bertoti, Z. Kantor, Z. Geretovszky, Excimer laser processing of indium-tin-oxide films: an optical investigation, J. Appl. Phys. 78 (1995) 6211–6219.